Toward understanding and optimizing Au-hyperdoped Si infrared photodetectors

S. Q. Lim, C. T.-K. Lew, P. K. Chow, J. M. Warrender, J. S. Williams, and B. C. Johnson

View Online   Export Citation   CrossMark

ARTICLES YOU MAY BE INTERESTED IN

AIP Publishing

Toward understanding and optimizing Au-hyperdoped Si infrared photodetectors

View Online   Export Citation   CrossMark

S. Q. Lim,[1,a] (iD) C. T.-K. Lew,[2] P. K. Chow,[3] J. M. Warrender,[3] J. S. Williams,[1] and B. C. Johnson[2] (iD)

AFFILIATIONS

[1] Research School of Physics, The Australian National University, Canberra, ACT 2601, Australia
[2] Centre for Quantum Computing and Communication Technology, School of Physics, University of Melbourne, Victoria 3010, Australia
[3] U.S. Army ARDEC-Benet Labs, Watervliet, New York 12189, USA

[a] Author to whom correspondence should be addressed: qi.lim@anu.edu.au

ABSTRACT

Au-hyperdoped Si absorbs near-infrared (NIR) light and recent efforts have successfully produced Si-based NIR photodetectors based on this property but with low detection efficiencies. Here, we investigate the differences between the optical and photocurrent properties of Au-hyperdoped Si. Although defects introduced during fabrication of these materials may not exhibit significant optical absorption, we show that they can produce a measurable photocurrent under NIR illumination. Our results indicate that the optimal efficiency of impurity-hyperdoped Si materials is yet to be achieved and we discuss these opportunities in light of our results. This work thus represents a step forward in demonstrating the viability of using impurity-hyperdoped Si materials for NIR photodetection.

In the last decade, there have been numerous works reporting on impurity-hyperdoped Si and its potential to be an attractive material for room temperature near-to-mid-infrared (N/MIR) detection, despite limited success to date.[1–5] Being a Si-based material, existing low cost and mature Si processing technologies can be leveraged and thus are of interest for telecommunications and imaging applications. Hyperdoping refers to the incorporation of electrically active impurities into Si at concentrations well beyond their equilibrium solid solubility limit ($>10^{19}$ cm^{-3}) and can be achieved by ion implantation followed by pulsed laser melting (PLM). The crystallinity of the material is recovered after PLM through liquid phase epitaxy, with the implanted impurity forming an intermediate impurity band in the Si bandgap.[6] Thus, by hyperdoping Si with deep level impurities, broad sub-bandgap absorption can occur.[6]

Near-infrared (NIR) absorption with impurity-hyperdoped Si has been demonstrated with chalcogens[1] and transition metal impurities such as Au,[2,7] Ti,[3] and V.[4] Figure 1 illustrates the discrete levels of the latter in Si in the dilute concentration regime.[8] When the impurity concentration exceeds the Mott limit ($\sim 6 \times 10^{19}$ cm^{-3}), an impurity band(s) forms from the corresponding discrete level,

resulting in broad sub-bandgap light absorption.[6] Upon hyperdoping with Au, for example, the NIR absorptance extends up to 2200 nm[2] and achieved a value of 20% at 1550 nm.[2,7] This is significantly greater than Si self-implanted[9] and PLM-processed materials, which strongly suggests that the NIR absorption arises from hyperdoped Si rather than process-induced defects. Furthermore, NIR Si photodetectors based on impurity-hyperdoped materials have recently been demonstrated[2,3] with some success. These are often Schottky or pn-junction type devices where a photocurrent is generated via an impurity band. At present, the quantum efficiency of such photodetectors tends to be lower than expected (<0.01%), indicating opportunities for further development.

In this work, we investigate limitations to Au-hyperdoped Si photodetectors and pathways to improving their quantum efficiency, in an effort to assess their potential as Si-based NIR detectors. In our previous work, we discovered high concentrations ($\sim 10^{14}$ cm^{-3}) of process-induced defects (from Au implantation and PLM) within the depletion layer of Au-hyperdoped Si photodiodes.[10] The most prominent defect, $E_1(0.35)$, is a deep electron trap located at 0.35 eV below the Si conduction band edge, shown in Fig. 1. It is well known from the literature that
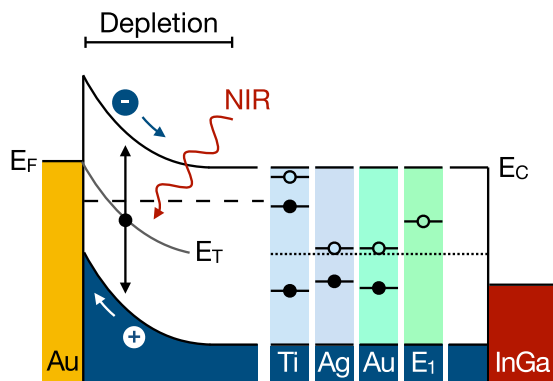
FIG. 1. Schematic of a reverse biased Au–Si Schottky diode illustrating a possible pathway for defect/impurity-assisted NIR photocurrent generation. To the right are the bandgap energy levels for a number of impurities[8] and a process-related defect level, $E_1(0.35)$ ($E_C - E_T = 0.35$ eV) in Si.[10] Open (closed) circles represent acceptor (donor) impurity states in the equilibrium dilute limit. High concentrations of deep level impurities from hyperdoping results in the formation of an impurity band from these discrete levels.

implantation-induced deep level defects in the Si bandgap can also result in N/MIR sub-bandgap absorption[9] and thus photo-carrier generation,[11,12] as illustrated in Fig. 1, although it is less than in hyperdoped Si.[1–3] Thus, we seek to determine what impact process-induced defects such as $E_1(0.35)$ have on the photoresponse of impurity-hyperdoped NIR photodetectors. To achieve this, we compare the optical and photocurrent properties for Au-hyperdoped Si and two other carefully designed control samples. We elucidate the extent of photocarrier generation at these process-induced defects. In light of these results, we then conclude by identifying possible pathways to improve upon present NIR Au-hyperdoped Si photodetectors.

Si-based NIR photodetectors were fabricated on ⟨100⟩ n-type Si substrates (P-doped, 1 Ω cm–10 Ω cm, and double-side polished with a measured $n_D \sim 2 \times 10^{15}$ cm^{-3}). Details on the device fabrication are described elsewhere.[10] Briefly, Au-hyperdoping was achieved with 300 keV Au implantation to a dose of 10^{15} cm^{-2} followed by PLM (as opposed to Au evaporation and PLM[7]). The two control samples consisted of a pristine Si substrate and an implanted (70 keV Si 10^{15} cm^{-2} followed by 300 keV Au 10^{10} cm^{-2}) and PLM processed substrate. These samples will be referred to as the Au-hyperdoped Si, pristine Si, and process control sample/diode, respectively. To form the photodiodes, front Au contacts (300 nm thick) with a diameter of 1 mm were deposited onto all three substrates by electron beam evaporation through a shadow mask. An Ohmic back contact was formed by applying InGa eutectic. Although this device design is clearly not optimized for photodetection, it was chosen for its simplicity and similarity to those used in the literature. Furthermore, we note that this choice of device design will not affect our discussions and subsequent conclusions as will be shown later, since these were based on relative differences between photocurrent signals of the three devices (not their absolute photocurrent).

Before further discussion, it should be noted that the process control sample was also implanted with Au (10^{10} cm^{-2}) as this was

found to significantly improve the rectification properties of the diode[10] (without which the sample behaves more like a resistor, with ~0.1 mA measured at ±0.5 V). As will be shown below, the NIR absorption of this sample was similar to that of a pristine Si sample. Thus, given the five orders of magnitude difference in Au concentration between the process control and Au-hyperdoped samples, we do not expect the low dose Au to have a significant impact on our results and subsequent discussions presented here. We further refer readers to our previous work[10] for a more in-depth treatment on the subject. We also note that the process-induced defect concentration in the depletion layer of this device was similar to that found in the Au-hyperdoped sample.[10]

Device schematics for the three devices are shown in Figs. 2(a)–2(c). Implantation energies were chosen for the Au and Si implants to obtain a peak ion range of 100 nm below the surface. After PLM, the Au-hyperdoped layer is around 250 ± 10 nm thick, within which the Au concentration exceeds 10^{19} cm^{-3} and peaks at 10^{20} cm^{-3} at around 100 ± 10 nm below the surface, as presented elsewhere.[10] The Au concentration tail, however, extends deeper into the substrate. As a result, the Au-hyperdoped Si sample forms a non-abrupt vertical p$^+$n-junction, as it is expected that the Au-hyperdoping has inverted the surface Si layer to p-type[2,10,13] [Fig. 2(a)]. On the other hand, the
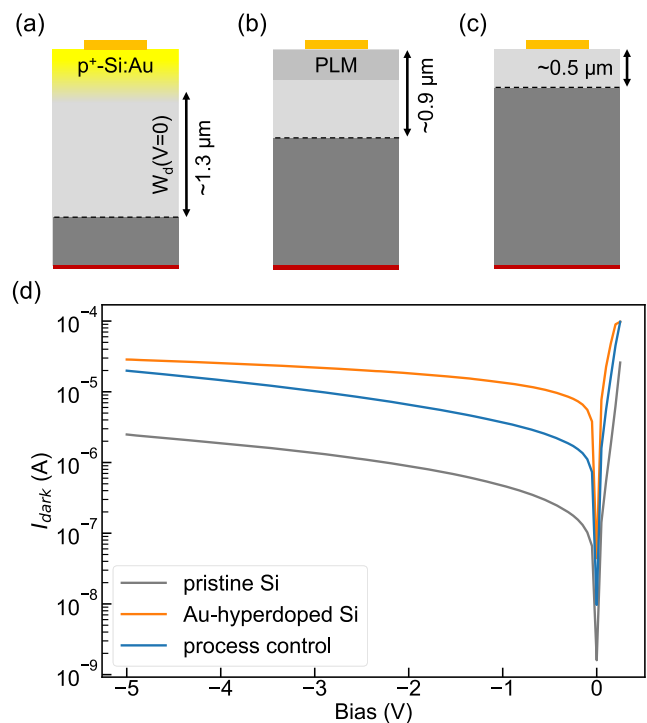
FIG. 2. Schematics of (a) the Au-hyperdoped Si device, similar to a graded p$^+$n-junction, and SBDs formed on the (b) process control and (c) pristine Si samples. The lighter gray regions indicate the depletion layer in the n-type Si at zero-bias [$W_d(V = 0)$], which will extend deeper into the substrate with reverse bias. The front Au and back InGa contacts are indicated in orange and red, respectively. (d) The dark I–V characteristics of these three devices show that they are rectifying diodes.

two other control samples behave as Schottky barrier diodes (SBD)[10] [Figs. 2(b) and 2(c)]. Dark current–voltage measurements (I–V) [shown in Fig. 2(d)] confirm that all devices are indeed rectifying diodes.

We calculated the zero-bias depletion widths of our devices through capacitance–voltage measurements (published elsewhere[10]) and found them to be $W_d(V = 0) \sim 0.5~\mu m$, $0.9~\mu m$, and $1.3~\mu m$ for the pristine, process control, and Au-hyperdoped Si samples, respectively. These are indicated in Figs. 2(a)–2(c). The depletion layer of our Au-hyperdoped Si diode begins at the metallurgical junction, where the substrate doping (n-type) and Au impurity (p-type) concentrations are equal (i.e., $n_D = n_{Au}$). Although the exact location of the junction is not known accurately [reflected by the indistinct junction depth in Fig. 2(a)], our Au concentration-depth profiling measurements[10] indicate that the Au concentration tail extends several hundreds of nanometers below the surface. The metallurgical junction where $n_{Au} = n_D$ is estimated to be ~340 nm below the surface based on Au diffusion kinetics. Thus, the Au-hyperdoped layer (~250 nm thick with $n_{Au} > 10^{19}~cm^{-3}$) is entirely confined within the p-type surface layer and does not overlap with the depletion layer. As for the process control and pristine Si samples, the depletion layer extends from the metal–semiconductor interface at the surface and thus includes the implanted and PLM layer, as shown in Figs. 2(b) and 2(c).

Prior to front contact formation, optical transmittance measurements were performed by Fourier Transform Infrared Spectroscopy (FTIR) using a Bruker VERTEX 80v vacuum FTIR spectrometer. Measurements were performed in the NIR range $(2500~cm^{-1}$–$14\,000~cm^{-1})$ with a CaF_2 beam splitter and a deuterated triglycine sulfate (DTGS) detector and averaged over 360 scans. Transmittance spectra were calculated by performing a Fourier transform on the (Mertz phase-corrected) interferogram using a Blackman–Harris three-term apodization scheme with a zero filling factor of two.

Photocurrent measurements were performed at room temperature by focusing a 1550 nm Thorlabs LPSC-1550-FC laser diode (P = 8 mW) onto an area on the samples adjacent to the front metallic contacts. A square wave generator modulated the laser output at a 200 Hz repetition rate. The diodes were connected to a 10 kΩ comparative resistor, a voltage source, and a SRS830 lock-in amplifier. The resulting change in the diode current (proportional to the voltage drop across the comparative resistor measured by the lock-in amplifier) due to illumination, ΔI (referred to as the "photocurrent" in this work), was measured under reverse bias between 0 V and −5 V.

The NIR transmittance spectra for all three samples are presented in Fig. 3(a). The process control spectrum displayed a small and uniform −0.5% offset in transmittance as compared to the pristine Si reference spectrum. We believe that this is an artifact most likely caused by changes in the sample reflectance due to PLM. Thus, the process control spectrum is used as a baseline for PLM processed materials, including our Au-hyperdoped Si sample.

In the Au-hyperdoped Si sample, a noticeable 2% decrease in transmittance (increase in absorption) at 1550 nm (0.80 eV) relative to the pristine Si sample was observed. As the photon energy increases, the transmittance decreases further, where a decrease of up to 4% was observed near the Si band edge at ~1115 nm (1.11 eV). This feature becomes more apparent in the
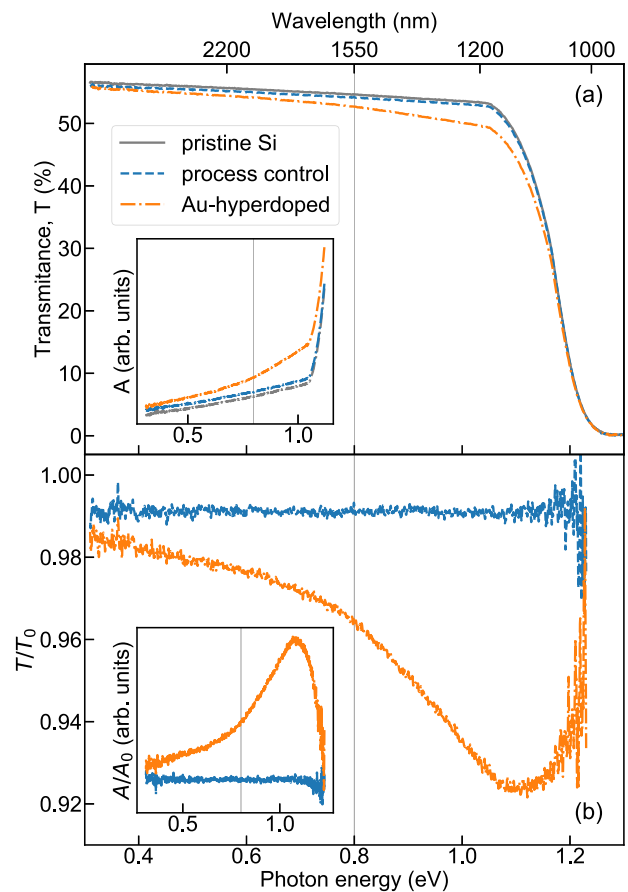

FIG. 3. (a) The transmittance as a function of wavelength for the Au-hyperdoped Si (orange), process control (blue), and pristine Si (gray). Measurements were performed before devices were fabricated with these materials. (b) The process control and Au-hyperdoped Si transmittance (T) are normalized against the pristine Si reference transmittance (T_0). The insets in (a) and (b) show the absorptance and normalized absorptance spectra of the same samples, respectively [calculated by $A = 2 - \log(T)$]. A vertical line indicates 1550 nm.

spectrum normalized against the pristine Si reference, T/T_0, plotted in Fig. 3(b).

It is more intuitive to examine the sample absorptance rather than transmission, as has been done elsewhere.[2,14] Here, we calculate the absorptance spectra, using Beer–Lambert's Law $A = 2 - \log(T)$, for all three samples, as shown in the insets of Fig. 3. We note that because partial reflection does occur at the surface of our samples, Beer–Lambert's equation cannot give us the absolute values to the absorptance, A (consequently A/A_0). Thus, the absorptance spectra are plotted in arbitrary units. Nevertheless, assuming a similar reflectance for all samples,[14] the line shape of these spectra is expected to agree with the true absorptance. From the calculated absorptance in the inset of Fig. 3(b), it is clear that Au-hyperdoping significantly enhances sub-bandgap absorption in Si, consistent with previous findings.[2,14,15] Importantly, the process control sample showed negligible sub-bandgap absorption.
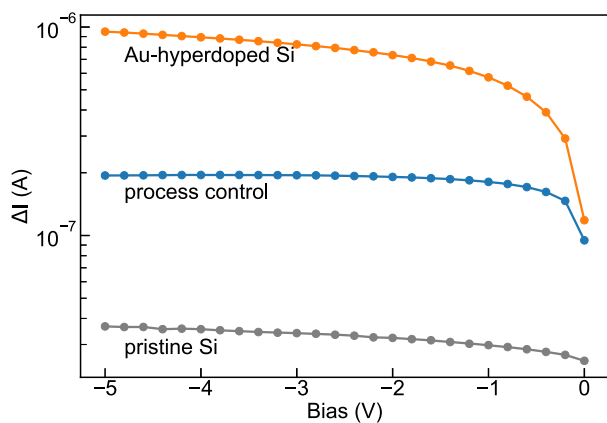
FIG. 4. Photocurrent in response to a 1550 nm excitation (ΔI) for the Au-hyperdoped Si, process control, and pristine Si diodes as a function of applied bias.

Therefore, the process-induced defects in this material are not effective at absorbing NIR light.

It is reasonable to anticipate that the Au-hyperdoped Si sample would thus exhibit a NIR photocurrent much superior to that of the process control and pristine Si samples. Surprisingly, this behavior was not observed. The photocurrent in response to 1550 nm excitation, ΔI, is plotted as a function of the reverse bias in Fig. 4. A small photocurrent that increases with reverse bias was measured for the pristine Si control SBD (~40 nA at −5 V). This behavior requires further investigation; however, we believe that it is most likely due to Si surface states.[16,17] Other possibilities are from deep level defects introduced during electron beam evaporation[18] and photoemission from extraneous Au adjacent to our contacts that may form on evaporation through a shadow mask.[19] We also rule out two-photon absorption, which is negligible in our experiment (~10^{-10}, see Appendix A in the supplementary material).

For the process control diode, ΔI was measured to be about five times larger than the pristine Si control (0.2 μA at −5 V), saturating when the reverse bias exceeds −1 V. This is despite having a comparable absorptance to the pristine sample (Fig. 3). We attribute this NIR photoresponse to process-induced defects, such as the $E_1(0.35)$ defect, which are present in the depletion layer of the device.[10] Therefore, the saturation effect observed here may be a result of the defect concentration as a function of depth.[10] We also note that the $E_1(0.35)$ defect has a photoionization energy comparable to the transition metal impurities (Fig. 1) and the bands expected to form in hyperdoped Si materials. It is therefore reasonable to assume that this defect may play a similar role in these devices.[11,12]

An additional fivefold increase in ΔI relative to the process control sample was observed in Au-hyperdoped Si (1 μA at −5 V). This is a much lower increase than might be expected from the absorptance spectra presented in Fig. 3. Since this device also contains process-induced defects in the substrate, we also expect that a component of the photocurrent arises from these defects similar to the process control device. However, unlike the process control, ΔI of the Au-hyperdoped Si diode increases monotonically with applied bias.

This is most likely because, as the reverse bias increases, the depletion layer extends slightly into the Au-hyperdoped layer. Although the one-sided nature of the junction implies that the depletion layer will extend much more toward the substrate, the slight extension toward the Au-hyperdoped layer is sufficient to increase the number of injected photo-carriers across the junction. Consequently, ΔI increases gradually with applied bias. This is very similar to observations reported in the literature for an essentially identical Au-hyperdoped Si photodiode (2 μA at −5 V).[2] Thus, a component of the photocurrent is generated by process-induced defects within the substrate, while a further enhancement is achieved through Au hyperdoping.

The Au-hyperdoped Si diode photocurrent is within the same order of magnitude as the process control diode. Given the trends observed in the absorptance data in Fig. 3 and the large differences between the Au impurity and $E_1(0.35)$ defect density (~10^{20} cm^{-3} and 10^{14} cm^{-3}, respectively),[10] it is reasonable to expect their photocurrents to differ by several orders of magnitude. However, this commonly used vertical p$^+$n-junction device structure[2] results in a NIR absorbing Au-hyperdoped layer (photo-carrier generating layer) that does not overlap with the device depletion layer (electric field region) [see Fig. 2(a)]. Thus, photo-carriers generated in the Au-hyperdoped layer will not be efficiently collected as a photocurrent at the device contacts, resulting in a much reduced ΔI.

Furthermore, preliminary calculations and experiments indicate that the carrier lifetime (τ) within the Au-hyperdoped Si layer is very short. We perform order of magnitude estimates of τ by first assuming that τ is similar for both electrons and holes and that the Au atoms residing outside the depletion layer are electrically neutral within the Si lattice. Following similar calculations put forth in Ref. 20, a carrier lifetime of τ = 10 ps is obtained (see Appendix B in the supplementary material for expanded calculations). This is in good agreement with carrier lifetime experiments performed on impurity-hyperdoped Si materials in the literature.[21,22] Indeed, these results are unsurprising since it is well known that heavy doping will inevitably result in carrier lifetime deterioration[19] and that Au is also an efficient non-radiative recombination center in Si.[8] As a consequence of short carrier lifetimes, the mean carrier diffusion length, $L = \sqrt{D\tau}$, will also be short and is approximately 60 nm in our experiment (where $D \approx 3$ cm^2/s[23]).[24] This is less than the distance between the front metallic contact and the Au concentration peak post-PLM (100 nm). As a result, photo-carrier transport is mostly constrained to within the Au-hyperdoped layer.

Finally, our results highlight two important issues, namely, the need for efficient collection of photo-carriers generated in the hyperdoped layer due to short lifetimes and the related requirement that the hyperdoped layer overlaps more completely with the depletion region for more efficient photodetection. Both of these may be addressed with a more sophisticated device design tailored to the constraints imposed by the implantation and PLM processes. More specifically, device optimization strategies that we are actively exploring include having lateral pn-junctions within the hyperdoped region with more closely spaced contacts to aid carrier collection and employing a MOS-capacitor type structure. Such optimization efforts are necessary to more adequately assess the commercial potential of impurity-hyperdoped Si diodes for NIR

photodetection. We further note that previous efforts in the literature targeted at improving the detection efficiencies of such materials mostly involve increasing the impurity concentration by increasing the implant dose,[2,5] which, in light of our results, might not be the best way forward, as it can sometime lead to additional unexpected complications during fabrication such as filamentary breakdown.[14,25] Alternative methods to hyperdope Si such as Au deposition onto the Si surface followed by PLM[7] may also present further opportunities to improve the quality of the device, although this will be limited by the maximum Au concentration that can be incorporated. Interestingly, such thin film Au-hyperdoped devices were found to have a very similar 1550 nm photocurrent (~1.2 μA) (published elsewhere) to what we report here and in Ref. 2. This is despite the difference in Au and defect concentrations between the thin film and our implanted samples and its more sophisticated detector design (vertical pn-junction, mesa structure with SiO_x passivation[7]), further emphasizing the need for more customized device optimization strategies tailored to the limitations of the material.

To conclude, we have investigated the optical and photocurrent properties of Au hyperdoped Si photodiodes. These were compared to pristine and implanted-PLM processed control diodes. The Au-hyperdoped and process control devices contain similar process-induced defects in the depletion region. Although the hyperdoped material displayed a significantly greater absorptance than both control samples, the photocurrent in this device did not show a similar trend. Likewise, the process control sample absorptance was similar to the pristine Si sample, but its photocurrent was within the same order of magnitude as the Au-hyperdoped sample. This disparity between our optical and photocurrent measurements strongly suggests that process-induced defects make a significant contribution to the photocurrent in both the process control and Au-hyperdoped devices. This also indicates that substantial gains to the Au-hyperdoped Si device can be made by strategically positioning the active device region within the hyperdoped layer. Thus, an enhanced quantum efficiency of Si-based NIR detectors may be achieved with modifications to the device architecture.

See the supplementary material for calculations on two-photon absorption (Appendix A) and expanded carrier lifetime calculations (Appendix B).

DATA AVAILABILITY

The data that support the findings of this study are available from the corresponding author upon reasonable request.

REFERENCES

[1] A. J. Said, D. Recht, J. T. Sullivan, J. M. Warrender, T. Buonassisi, P. D. Persans, and M. J. Aziz, Appl. Phys. Lett. **99**, 073503 (2011).

[2] J. P. Mailoa, A. J. Akey, C. B. Simmons, D. Hutchinson, J. Mathews, J. T. Sullivan, D. Recht, M. T. Winkler, J. S. Williams, J. M. Warrender, P. D. Persans, M. J. Aziz, and T. Buonassisi, Nat. Commun. **5**, 3011 (2014).

[3] E. García-Hemme, R. García-Hernansanz, J. Olea, D. Pastor, A. Del Prado, I. Mártil, and G. González-Díaz, Appl. Phys. Lett. **104**, 211105 (2014).

[4] E. García-Hemme, R. García-Hernansanz, J. Olea, D. Pastor, A. del Prado, I. Mártil, and G. González-Díaz, Appl. Phys. Lett. **103**, 032101 (2013).

[5] M. Wang, Y. Berencén, E. García-Hemme, S. Prucnal, R. Hübner, Y. Yuan, C. Xu, L. Rebohle, R. Böttger, R. Heller et al., Phys. Rev. Appl. **10**, 024054 (2018).

[6] W. Yang, J. Mathews, and J. S. Williams, Mater. Sci. Semicond. Process. **62**, 103 (2017).

[7] P. K. Chow, W. Yang, Q. Hudspeth, S. Q. Lim, J. S. Williams, and J. M. Warrender, J. Appl. Phys. **123**, 133101 (2018).

[8] K. Graff, Metal Impurities in Silicon-Device Fabrication (Springer Science & Business Media, 2013), Vol. 24.

[9] H. Y. Fan and A. K. Ramdas, J. Appl. Phys. **30**, 1127 (1959).

[10] S. Q. Lim, C. T.-K. Lew, P. K. Chow, J. M. Warrender, J. S. Williams, and B. C. Johnson, J. Appl. Phys. **126**, 224502 (2019).

[11] A. P. Knights, A. A. House, R. MacNaughton, and F. Hopper, Optical Fiber Communication Conference (Optical Society of America, 2003), p. FJ3.

[12] M. W. Geis, S. J. Spector, M. E. Grein, R. T. Schulein, J. U. Yoon, D. M. Lennon, S. Deneault, F. Gan, F. X. Kaertner, and T. M. Lyszczarz, IEEE Photonics Technol. Lett. **19**, 152 (2007).

[13] M. Valdinoci, L. Colalongo, A. Pellegrini, and M. Rudan, IEEE Trans. Electron Devices **43**, 2269 (1996).

[14] W. Yang, A. J. Akey, L. A. Smillie, J. P. Mailoa, B. C. Johnson, J. C. McCallum, D. Macdonald, T. Buonassisi, M. J. Aziz, and J. S. Williams, Phys. Rev. Mater. **1**, 074602 (2017).

[15] N. Ferdous and E. Ertekin, AIP Adv. **8**, 055014 (2018).

[16] W. Müller and W. Mönch, Phys. Rev. Lett. **27**, 250 (1971).

[17] W. Müller and W. Mönch, Phys. Status Solidi A **24**, 197 (1974).

[18] F. D. Auret and P. M. Mooney, J. Appl. Phys. **55**, 988 (1984).

[19] S. M. Sze and K. K. Ng, Physics of Semiconductor Devices, 3rd ed. (John Wiley & Sons, 2006), p. 680.

[20] G. Güttler and H. J. Queisser, Energy Convers. **10**, 51 (1970).

[21] S. Dissanayake, P. Chow, S. Q. Lim, M. Wilkins, E. Dumitresc, W. Yang, Q. Hudspeth, J. Krich, J. Williams, J. Warrender, and M.-J. Sher, in Conference on Lasers and Electro-Optics, 2018.

[22] M.-J. Sher, C. B. Simmons, J. J. Krich, A. J. Akey, M. T. Winkler, D. Recht, T. Buonassisi, M. J. Aziz, and A. M. Lindenberg, Appl. Phys. Lett. **105**, 053905 (2014).

[23] A. P. Silard and M. J. Duţă, J. Appl. Phys. **62**, 3809 (1987).

[24] Minority carriers will have values for τ and L less than those calculated for holes. Readers are also referred to Appendix B for calculations concerning E_1(0.35) in the substrate.

[25] J. Mathews, A. J. Akey, D. Recht, G. Malladi, H. Efstathiadis, M. J. Aziz, and J. M. Warrender, Appl. Phys. Lett. **104**, 112102 (2014).

Author/s:
Lim, SQ; Lew, CT-K; Chow, PK; Warrender, JM; Williams, JS; Johnson, BC

Title:
Toward understanding and optimizing Au-hyperdoped Si infrared photodetectors

Date:
2020-06-01

Citation:
Lim, S. Q., Lew, C. T. -K., Chow, P. K., Warrender, J. M., Williams, J. S. & Johnson, B. C. (2020). Toward understanding and optimizing Au-hyperdoped Si infrared photodetectors. APL MATERIALS, 8 (6), https://doi.org/10.1063/5.0010083.

Persistent Link:
http://hdl.handle.net/11343/252479

File Description:
Published version
License: